

Conservative multirate multiscale simulation of multiphase flow in heterogeneous porous media

Ludovica Delpopolo Carciopolo^{a,*}, Luca Formaggia^a, Anna Scotti^a, Hadi Hajibeygi^b

^a*MOX, Dipartimento di Matematica, Politecnico di Milano, Via Bonardi 9, 20133 Milano, Italy*

^b*Faculty of Civil Engineering and Geosciences, Department of Geoscience and Engineering, Delft University of Technology, Stevinweg 1, 2628CV Delft, Netherlands*

Abstract

Accurate and efficient simulation of multiphase flow in heterogeneous porous media motivates the development of space-time multiscale strategies for the coupled nonlinear flow (pressure) and saturation transport equations. The flow equation entails heterogeneous high-resolution (fine-scale) coefficients and is global (elliptic or parabolic). The time-dependent saturation profile, on the other hand, may exhibit sharp local gradients or discontinuities (fronts) where the solution accuracy is highly sensitive to the time-step size. Therefore, accurate flow solvers need to address the multiscale spatial scales, while advanced transport solvers need to also tackle multiple time scales. This paper presents the first multirate multiscale method for space-time conservative multiscale simulation of sequentially coupled flow and transport equations. The method computes the pressure equation at the coarse spatial scale with a multiscale finite volume technique, while the transport equation is solved by taking variable time-step sizes at different locations of the domain. At each coarse time step, the developed local time-stepping technique employs an adaptive recursive time step refinement to capture the fronts accurately. The applicability (accuracy and efficiency) of the method is investigated for a wide range of two-phase flow simulations in heteroge-

*Corresponding author.

Email addresses: Ludovica.Delpopolo@polimi.it (Ludovica Delpopolo Carciopolo), Luca.Formaggia@polimi.it (Luca Formaggia), Anna.Scotti@polimi.it (Anna Scotti), H.Hajibeygi@TUDelft.nl (Hadi Hajibeygi)

neous porous media. For the studied cases, the proposed method is found to provide 3 to 4 times faster simulations. Therefore, it provides a promising strategy to minimize the tradeoff between accuracy and efficiency for field-scale applications.

Keywords: Conservative multirate methods, Iterative multiscale methods, Multiscale finite-volume method, Multiphase flow, Porous media

1. Introduction

Efficient and accurate simulation of multiphase flow in natural heterogeneous porous media is challenging. Parameter heterogeneity strongly affects the flow field, which needs to be adequately resolved by the grid. In addition, the presence of dissimilar and nonlinear phase velocities can restrict the time step size to achieve accurate transport solutions. This leads to computationally inefficient simulations, specially for field-scale applications.

Multiscale finite element [1, 2, 3] and finite-volume [4, 5] methods have been developed to reduce computational costs by solving coarser-resolution spatial systems. The coarse-scale system entries are obtained by introducing locally-computed basis functions. As such, they have been developed conveniently for elliptic [6, 7, 8, 9] and parabolic [10, 11] flow equations within sequential [12, 13, 14, 15, 16] and fully implicit [17, 18] multiphase simulation frameworks. Recent advances include extensions to geothermal flows [19, 20] and fractured heterogeneous media [21, 22, 23, 24, 25, 26]. Note that the difference between the multiscale finite volume and finite element methods is in the coarse scale system solution strategies. In particular, they both use the same basis functions to map the fine and coarse scale solutions. As such, the development of either of them leads to advancement of the alternative method too. An essential feature of this class of multiscale simulation is that it can be formulated algebraically for two-level [27, 28, 29] and dynamic multilevel [30] simulations, in which the difference between the finite-element and finite-volume approaches is only in the choice of the restriction operator.

In sequential simulation of multiphase flow, once the pressure solution is obtained, a hyperbolic saturation equation needs to be solved. Due to the sharp saturation fronts, small time steps are often required to achieve the desired accuracy. Any local time-step size restrictions results in global restriction of the time-step size. As such, accurate solutions can only be achieved if small time step sizes are taken everywhere in the domain. This imposes a sig-

nificant challenge in real-field applications, in which simulation efficiency is a crucial objective for timely decisions [31, 32]. This challenge can be solved by multirate techniques [33]. Multirate methods achieve the required accuracy with employing the refined time step only locally. More precisely, they allow for a flexible selection of time-step size within the domain based on the flow characteristics. They are different, yet complementary, to Adaptive Implicit (AIM) [34, 35, 36, 37, 38, 39] and potential ordering [40] methods, which enhance the simulation stability by combining explicit-implicit integration strategies. In multirate methods, instead, the system is subdivided into two subsystems: one containing the active (fast) components that need small time steps, and the other formed by the latent (slow) components, where larger time steps can be used.

In the early developments of the multirate methods, the subsystems were characterized and partitioned based on the most-updated available solution [41]. Later extensions include a self-adjusting strategy to select the fast components automatically [42]. Note that most of the developments within the multirate literature address only hyperbolic wave equations [43, 44]. Furthermore, they mainly implement non-conservative procedures, which can lead to stability issues when applied to coupled flow-transport systems. Recently, conservative multirate methods have been introduced for hyperbolic transport (wave) equations [45, 46]. Of particular interest is the development of a conservative multirate method for transport in heterogeneous porous media integrated within the nonlinear multiphase flow simulation.

In this paper, we present a novel conservative multirate multiscale method for multiphase flow simulation in heterogeneous porous media. The pressure-saturation coupling is treated via the sequential implicit formulation [47]. Pressure is computed with the iterative multiscale finite volume method [29] until the desired accuracy is reached. Then, locally conservative velocity is obtained by solving pressure equations on multiscale coarse elements, subject to Neumann flux conditions. This multiscale velocity field is used to solve the saturation equation with a multirate method up to a given accuracy. The multirate method employs, initially, a coarse-scale time step everywhere in the domain to estimate an updated saturation field. Then, the high sensitive (fast dynamics) zones are detected using an error estimate. Only for these zones the saturation will be recomputed with a smaller time step sizes. The integration of fast and slow zones is carried out using a flux-constrained formulation, in order to guarantee local mass conservation. This combination of space-time multiscale strategies for flow and transport aims at minimizing

the tradeoff between accuracy and efficiency by adapting both space and time computational grids.

The local-global concept of multiscale methods for pressure equation makes them amenable for parallel processing. Development of a parallel multirate method for transport equation, however, requires an efficient load balancing strategy when only on a small sub-domain is solved with refined time steps. The focus of this work, however, is on serial simulation strategy. Development of an efficient parallel multirate simulation strategy is out of the scope of this paper.

The accuracy and efficiency of the proposed method are investigated for several test cases. In particular, the computational complexity reduction is estimated based on the size of the refined time-step zones as well as the count of the nonlinear iteration loops. These are relevant performance indicators for the developed research code, which is based on a high-level programming language.

The paper is organized as follows. The governing equations for multiphase flow in porous media at continuum (Darcy's) scale are presented in Section 2. In Section 3, space and time discretization schemes adopted for both flow and transport equations are presented, and the multiscale multirate method for sequential implicit multiphase flow is described. Section 4 contains several numerical tests that demonstrate the effectiveness of the approach, followed by a concluding section.

2. Governing equations

Let N_p be the number of phases present in the porous medium. Given a d -dimensional domain $\Omega \subset \mathbb{R}^d$, mass balance for an incompressible phase α reads

$$\frac{\partial}{\partial t} (\phi S_\alpha) + \nabla \cdot \mathbf{u}_\alpha = \mathbf{q}_\alpha, \quad \alpha \in \{\mathbf{1}, \dots, \mathbf{N}_p\}, \quad (1)$$

where ϕ is the porosity, S_α the saturation, \mathbf{u}_α the phase Darcy velocity and q_α the source term. Neglecting gravitational and capillary effects, the Darcy phase velocity is given by

$$\mathbf{u}_\alpha = -\lambda_\alpha \mathbf{K} \cdot \nabla p \quad \text{in } \Omega, \quad (2)$$

where p is the pressure and $\lambda_\alpha = k_{r\alpha}/\mu_\alpha$ is the phase mobility, i.e., the ratio of the relative permeability $k_{r\alpha}$ (a function of the phase saturations) and the phase viscosity μ_α [48]. The permeability \mathbf{K} is a heterogeneous symmetric

positive definite tensor. In the numerical experiments of this paper, it is considered to be isotropic, i.e. $\mathbf{K} = K\mathbf{I}$, with \mathbf{I} the identity tensor. Note that the constraint $\sum_{i=1}^{N_p} S_i = 1$ holds, i.e. the pore space is completely filled with fluid phases.

For the considered incompressible system, the pressure equation reads

$$-\nabla \cdot (\lambda_t \mathbf{K} \cdot \nabla p) = q_t \quad \text{in } \Omega, \quad (3)$$

which is obtained by summing all the phase balance equations [49]. Here, $\lambda_t = \sum_{i=1}^{N_p} \lambda_i$ is the total mobility and $q_t = \sum_{i=1}^{N_p} q_i$ the total source term. Total velocity is obtained as $\mathbf{u}_t = -\lambda_t \mathbf{K} \cdot \nabla p$ and, consequently, the phase velocities are computed by $\mathbf{u}_\alpha = f_\alpha \mathbf{u}_t$. The fractional flow function is found by $f_\alpha = \lambda_\alpha / \lambda_t$. Following this terminology, one can re-write the $(N_p - 1)$ saturation equations (1) as

$$\phi \frac{\partial S_\alpha}{\partial t} + \nabla \cdot (f_\alpha \mathbf{u}_t) = f_\alpha q_t, \quad \alpha \in \{1, \dots, N_{p-1}\}, \quad (4)$$

where, for simplicity, porosity is considered constant. The N_p -th saturation is computed via $S_{N_p} = 1 - \sum_{i=1}^{N_p-1} S_i$. Equations (3) and (4) are coupled, due to the dependency of the phase mobilities to the saturations and the velocity to the pressure.

The boundary $\partial\Omega$ of the domain Ω is split into non-overlapping Dirichlet Γ_D and Neumann Γ_N parts, where the measure of Γ_D is non-zero. The boundary conditions for the pressure equations thus read

$$\begin{aligned} p &= p_D && \text{on } \Gamma_D \\ (\lambda_t \mathbf{K} \cdot \nabla p) \cdot \mathbf{n} &= \mathbf{u}_t \cdot \mathbf{n} = b && \text{on } \Gamma_N, \end{aligned}$$

where \mathbf{n} is the outwardly oriented unitary vector normal to $\partial\Omega$, while p_D and b are given data. Boundary conditions for the transport equations should be defined only at the inflow (upwind) boundary $\Gamma_- = \{x \in \partial\Omega : \mathbf{u}_t \cdot \mathbf{n} < 0\}$, i.e.,

$$S_\alpha = \bar{S}_\alpha \quad \text{on } \Gamma_- \quad \alpha \in \{1, \dots, N_{p-1}\}, \quad (5)$$

and \bar{S}_α is the known Dirichlet value. In addition, S_α^0 is a given initial solution at the initial time $t = 0$, i.e.,

$$S_\alpha = S_\alpha^0 \quad \text{in } \Omega \quad \alpha \in \{1, \dots, N_{p-1}\}. \quad (6)$$

With the stated boundary and initial conditions, equations (3) and (4) form a well-posed coupled system for N_p unknowns.

3. Multirate multiscale approach

Following the sequential simulation strategy [50], the solution at the current time step t^n is used to find the solution at t^{n+1} by first solving the pressure equation, i.e.,

$$-\nabla \cdot (\lambda_t(S_\alpha^n) \mathbf{K} \cdot \nabla p^{n+1}) = q_t \quad \text{in } \Omega. \quad (7)$$

Then, the total velocity is computed as

$$\mathbf{u}_t^{n+1} = -\lambda_t \mathbf{K} \cdot \nabla p^{n+1}. \quad (8)$$

Finally, the saturation values are found by solving

$$\phi \frac{S_\alpha^{n+1} - S_\alpha^n}{\Delta t} + \nabla \cdot (f_\alpha^{n+1} \mathbf{u}_t^{n+1}) - f_\alpha^{n+1} q_t = 0 \quad \text{in } \Omega, \quad (9)$$

where Δt is the time step size, and the superscript n and $n + 1$ indicate quantities at the current and next time steps, respectively.

The fine-scale (in space) discrete system for the pressure is obtained using a finite-volume-based two-point-flux-approximation scheme. Let \mathcal{T}_h be a fine-scale mesh formed by rectangular (or hexahedral in 3D) control volumes $K \in \mathcal{T}_h$. The set of faces e of a generic element K is denoted by \mathcal{E}_K . The flow equation is then discretized as

$$-\sum_{e_{KL} \in \mathcal{E}_K} F_{e_{KL}} = |K| q_{t_K} \quad \forall K \in \mathcal{T}_h, \quad (10)$$

where $|K|$ is the measure (volume for three-dimensional elements, area in two-dimensional elements) of K , e_{KL} the face shared with the adjacent element L , and the numerical flux $F_{e_{KL}}$ is

$$F_{e_{KL}} = \tau_{K|L} (p_L - p_K) \quad \forall e_{KL} \in \mathcal{E}_K. \quad (11)$$

Here, p_K and p_L are the constant pressure approximation in cell K and its neighboring cell, respectively. The interface transmissibility $\tau_{K|L}$ is taken as the harmonic average of the permeability of the two neighboring cells, i.e.

$$\tau_{K|L} = |e_{KL}| \left(\frac{d_{Ke_{KL}} \mathbf{K}_K^{-1}}{\lambda_{t_K}} + \frac{d_{Le_{KL}} \mathbf{K}_L^{-1}}{\lambda_{t_L}} \right)^{-1} \quad (12)$$

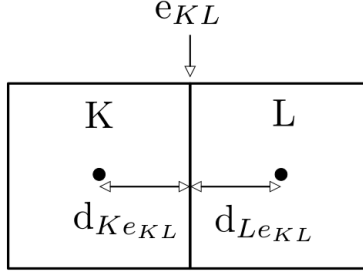


Figure 1: Example of a control volume K and the neighboring cell L .

where $|e_{KL}|$ is the measure of face e_{KL} , while $d_{Ke_{KL}}$ and $d_{Le_{KL}}$ are the distance between the face e_{KL} and the center of cells K and L , respectively, as shown in Figure 1.

The discrete saturation equation for phase α reads

$$\phi \frac{S_{\alpha K}^{n+1} - S_{\alpha K}^n}{\Delta t} |K| + \sum_{e_{KL} \in \mathcal{E}_K} \tilde{F}_{e_{KL}, \alpha}^{n+1} u_{t_{KL}} - \tilde{F}_{K, \alpha}^{n+1} q_{t_K} = 0 \quad \forall K \in \mathcal{T}_h. \quad (13)$$

The discrete flux $\tilde{F}_{e_{KL}, \alpha}^{n+1}$ is computed based on a first-order upwind method, as follows. Let $S_{\alpha U}^{n+1}$ and $S_{\alpha D}^{n+1}$ be the upstream and downstream saturation values at e_{KL} with respect to the total velocity. The discrete flux reads

$$\tilde{F}_{e_{KL}, \alpha}^{n+1} = \begin{cases} f_{\alpha}(S_{\alpha U}^{n+1}) & \text{if } u_{T_{KL}} > 0, \\ f_{\alpha}(S_{\alpha D}^{n+1}) & \text{otherwise,} \end{cases} \quad (14)$$

where $u_{T_{KL}}$ is the velocity at face e_{KL} . The source term flux, $\tilde{F}_{K, \alpha}^{n+1}$, is computed (for production cells) based on the saturation of the cell. Note that the fractional flow f_{α} is a nonlinear function of the saturation, so an iterative strategy based on Newton linearization is used to solve the nonlinear transport equation (13). Since the flux function can be non-convex, to ensure convergence, the modified Newton method is employed [51].

For efficient and accurate simulation of the coupled flow-transport equations, we present a multirate multiscale method. As shown in Figure 2, the multiscale finite volume approach is employed to solve the flow equation at the coarse-scale. The accuracy of the pressure solution is controlled by the iterative multiscale procedure. Local mass conservative velocity is computed

once the pressure solution is obtained. This conservative velocity is then used to solve the saturation transport equation with the developed conservative multirate method. More details are provided in the following sub-sections.

3.1. The multiscale method for the pressure equation

The multiscale method considers two sets of coarse grids, denoted as primal and dual coarse grids, built on a given fine-scale computational grid. The primal coarse grid defines the control volumes to solve the pressure equation at the coarse scale. The dual grid, on the other hand, provides the local supports for the computation of multiscale basis functions. Figure 3 illustrates the construction of the coarse grids. Other special local functions, for instance well-functions near fine-scale source terms, can also be introduced in the dual coarse grids [29].

Let M and N be the number of coarse and dual coarse cells, respectively. The multiscale method provides an approximate fine-scale solution p' , using

$$p_f(\mathbf{x}) \approx p'(\mathbf{x}) = \sum_{k=1}^M \Phi_k(\mathbf{x}) \bar{p}_k \quad (15)$$

expression. Here, p_f is the fine-scale reference solution, and Φ_k and \bar{p}_k are, respectively, the basis function and coarse-scale solution associated to the coarse node k . The former is found by assembling specially constructed local basis functions associated to that node in the dual coarse cells. More precisely, $\Phi_k(\mathbf{x}) = \sum_{h=1}^N \Phi_k^h(\mathbf{x})$, where $\Phi_k^h(\mathbf{x})$ is obtained by solving

$$\begin{cases} -\nabla \cdot (\lambda_t \mathbf{K} \cdot \nabla \Phi_k^h) = 0 & \text{in } \tilde{\Omega}^h \\ -\nabla_{\parallel} \cdot (\lambda_t \mathbf{K} \cdot \nabla \Phi_k^h)_{\parallel} = 0 & \text{on } \partial \tilde{\Omega}^h \\ \Phi_k^h(\mathbf{x}_i) = \delta_{ik} & \forall \mathbf{x}_i \in \{1, \dots, M\} \end{cases} \quad (16)$$

on each dual-coarse cell. Here, subscript \parallel denotes a reduced problem along the tangential direction of the dual-coarse cell boundary. Note that, by construction, Φ_k^h is zero outside $\tilde{\Omega}^h$.

These basis functions can be computed directly from the matrix of the fine-scale pressure system after some algebraic operations [29]. They can be collected as columns of the prolongation matrix \mathcal{P} , i.e.,

$$\mathcal{P} = [\Phi^1 \quad \Phi^2 \quad \dots \quad \Phi^N]. \quad (17)$$

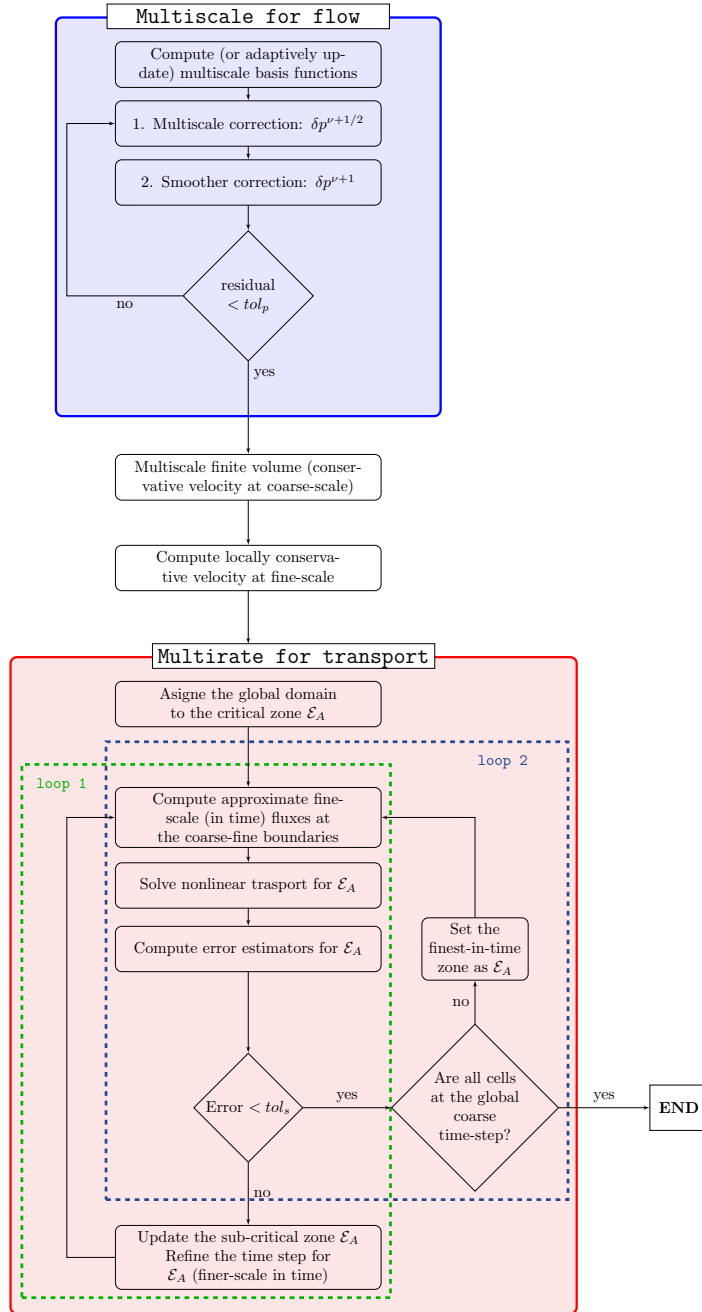


Figure 2: Description of the multirate multiscale algorithm for a time step.

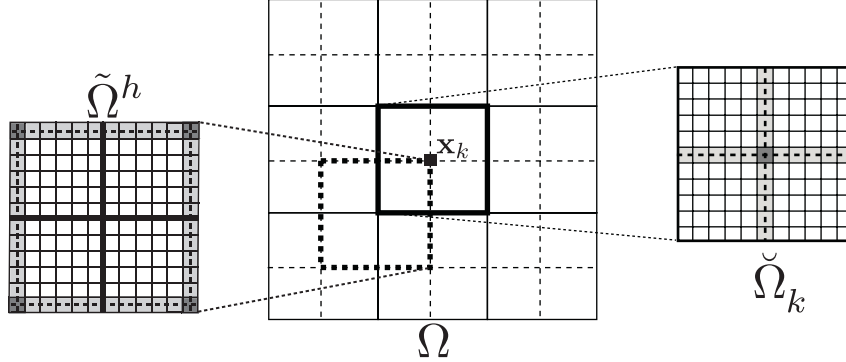


Figure 3: Illustration of the multiscale grids. Shown on the right and left are a coarse cell $\tilde{\Omega}_k$ and a dual-coarse cell $\tilde{\Omega}^h$, respectively.

which maps the coarse-scale solution to the fine grid. The restriction operator \mathcal{R} , maps fine to coarse scale, is defined as

$$\mathcal{R}(i, j) = \begin{cases} 1 & \text{if fine cell } j \text{ is in coarse cell } i, \\ 0 & \text{otherwise.} \end{cases} \quad (18)$$

More details can be found in [29].

From the algebraic pressure equation at fine-scale $Ap_f = b$, the multi-scale operator can be stated as $M_{MSFV}^{-1} = \mathcal{P}(\mathcal{R}A\mathcal{P})^{-1}\mathcal{R}$. Furthermore, the iterative multiscale procedure reads

1. Multiscale stage: $\delta p^{\nu+\frac{1}{2}} = p^{\nu+\frac{1}{2}} - p^\nu = M_{MSFV}^{-1} r^\nu$;
2. Smoothing stage: $\delta p^{\nu+1} = p^{\nu+1} - p^{\nu+\frac{1}{2}} = M_{ILU(0)}^{-1} r^{\nu+\frac{1}{2}}$;

where the residual vector r is updated using the latest available pressure, e.g. $r^{\nu+k} = b - Ap^{\nu+k}$. Steps 1 and 2 are repeated until the norm of the residual is below the desired threshold. Note that an ILU(0) factorization of the fine-scale matrix A is adopted in the smoothing stage, as it has been found to be an effective choice [29]. In addition, before entering this iterative procedure, for the fine-scale source terms the initial guess p^ν is improved by

$$p^{\nu'} = p^\nu + M_W^{-1} r^\nu, \quad (19)$$

where $p^{\nu'}$ is the improved initial guess and M_W^{-1} is an adaptive local block-solver which acts only on dual-coarse cells with nonzero fine-scale source terms. This can be seen as a form of well function [52]. Once the pressure is

obtained, an additional multiscale stage is employed to obtain a coarse-scale conservative velocity field. Local pressure equations on the primal coarse cells are solved, subject to the velocity computed from the multiscale approximate pressure field. This stage produces a fine-scale locally conservative velocity which is then used to update the saturation equations [5].

3.2. Conservative multirate method for the transport equation

The conservative multirate method for efficient solution of the saturation equation (9) is developed and presented in this section. Note that the saturation equation is nonlinear hyperbolic equation whose solution may exhibit highly localized variations and fronts. The multirate method adopts different time-step sizes in different parts of the spatial domain to increase computational efficiency while preserving accuracy. The proposed method is based on a flux partitioning strategy to maintain local mass conservation.

The multirate procedure can be summarized as follows: given the solution at time t^n , first an approximate solution at time t^{n+1} is computed for all cells using the coarse-scale time-step size Δt . This means that all cells will be initially assigned to the set of the critical zone \mathcal{E}_A , and thus

$$S_{\alpha_K}^{n+1} = S_{\alpha_K}^n - \frac{1}{\phi|K|} \sum_{e_{KL} \in \mathcal{E}_K} F_{e_{KL},\alpha}^{n+1} u_{t_{KL}}^{n+1} - \frac{1}{\phi|K|} F_K^{n+1} q_{t_K}^{n+1} \quad (20)$$

where

$$F_{e_{KL},\alpha}^{n+1} = \begin{cases} \Delta t f_\alpha(S_{\alpha_U}^{n+1}) & \text{if } u_{T_{KL}}^{n+1} > 0, \\ \Delta t f_\alpha(S_{\alpha_D}^{n+1}) & \text{otherwise.} \end{cases} \quad (21)$$

The value of the numerical fluxes at all cell interfaces e_{KL} is then checked, using an appropriate error estimator η_{KL} that will be detailed later on. If a flux is rejected on the basis of the error estimator, i.e. if the error estimate is greater than a given tolerance, cells K and L are added to the new set \mathcal{E}_A . Accordingly, for each cell K the set of active fluxes (where the flux does not satisfy the error criterion) and the set of fluxes at the interface between fine and coarse regions are defined as

$$\begin{aligned} \mathcal{E}_{K_A} &= \{\text{set of faces of the element } K : \eta_{KL} > \text{tol } \forall e_{KL} \in \mathcal{E}_K\}, \\ \mathcal{E}_{K_L} &= \{\text{set of faces of the element } K : \eta_{KL} \leq \text{tol } \forall e_{KL} \in \mathcal{E}_K\}. \end{aligned}$$

Solution in the cells belonging to \mathcal{E}_A will be recomputed (locally) with a smaller time step. This local solution will be obtained using an approximate

discrete flux as Neumann condition at the boundary of the refined zone. The Neumann value is obtained by scaling the coarse-scale fluxes by the ratio of the refined and the coarse time step. This scaling guarantees mass conservation of the solution at the global coarse time step. For example, if the refinement ration is 2, the saturation in the boundary cells between fine and coarse region is updated as

$$S_{\alpha_K}^{n+\frac{1}{2}} = S_{\alpha_K}^n - \frac{1}{\phi|K|} \sum_{e_{KL} \in \mathcal{E}_{K_L}} \frac{1}{2} F_{e_{KL}, \alpha}^{n+1} u_{t_{KL}}^{n+1} - \frac{1}{\phi|K|} \sum_{e_{KL} \in \mathcal{E}_{K_A}} F_{e_{KL}, \alpha}^{n+\frac{1}{2}} u_{t_{KL}}^{n+1} - \frac{1}{\phi|K|} F_{K, \alpha}^{n+\frac{1}{2}} q_{t_K}^{n+\frac{1}{2}}.$$

Here, $F_{e_{KL}}^{n+1}$ and $u_{t_{KL}}^{n+1}$ are frozen, since they are computed based on the coarse time step, and the factor $\frac{1}{2}$ indicates the ratio of the refined to the coarse time step size. If the updated fluxes based on $S_{\alpha}^{n+\frac{1}{2}}$ are all accepted, the final solution at time t_{n+1} reads

$$S_{\alpha_K}^{n+1} = S_{\alpha_K}^{n+\frac{1}{2}} - \frac{1}{\phi|K|} \sum_{e_{KL} \in \mathcal{E}_{K_L}} \frac{1}{2} F_{e_{KL}, \alpha}^{n+1} u_{t_{KL}}^{n+1} - \frac{1}{\phi|K|} \sum_{e_{KL} \in \mathcal{E}_{K_A}} F_{e_{KL}, \alpha}^{n+1} u_{t_{KL}}^{n+1} - \frac{1}{\phi|K|} F_{K, \alpha}^{n+1} q_{t_K}^{n+1}.$$

The example above is a simple case where just one refinement took place, i.e., the ratio of the coarse to fine time step was 2. However, the method has been extended to deal with an arbitrary level of refinements until the desired flux quality is reached. Therefore, a self-adjusting strategy is developed, where the sub-critical zones are updated continuously until all fluxes satisfy the quality threshold criterion. The method, thus, entails two main loops. Loop 1 detects and integrates the sub-critical regions until the flux quality check is satisfied. The time-step in each new sub-critical zone is divided (successively) by 2. Loop 2 advances the sub-critical zones in time, until the global time-step synchronization takes place. Figure 4 illustrates a schematic example of how the two loops perform. The thick lines represent the sub-critical zones \mathcal{E}_A and the highlighted sub-critical zones indicate cells where the transport equation has been solved either for refinement (Loop 1) or time advancing (Loop 2) stages.

The flux quality is verified with a-posteriori error estimator, originally derived in [53]. It is based on the difference of fluxes at the current and

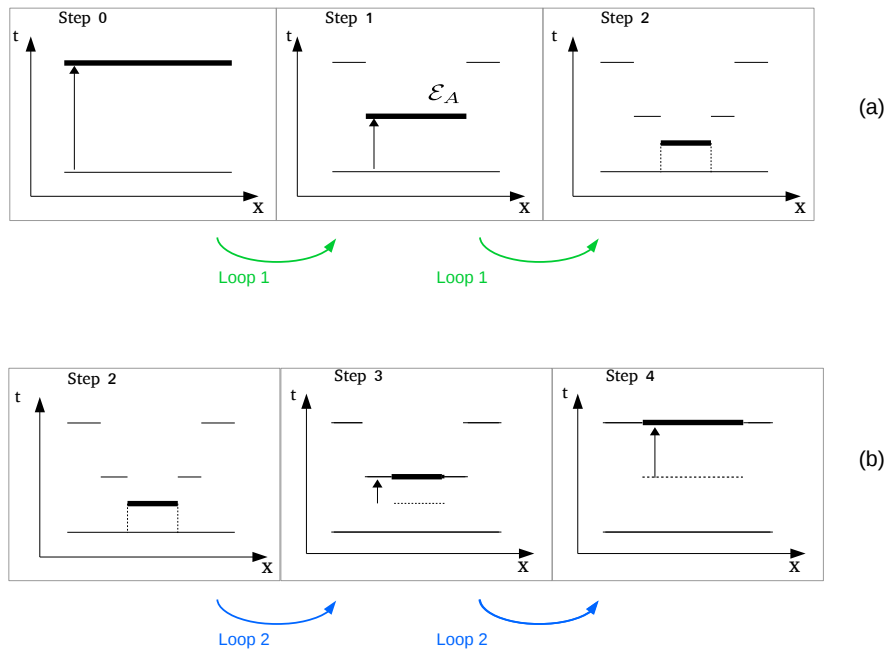


Figure 4: Schematic illustration of the integration in time with the multirate strategy for a global time step. In row (a) Loop 1 has been applied to refine in time until the flux quality is satisfied locally. In row (b) Loop 2 is employed to advance the sub-critical zones in time until synchronization with the global coarse time is reached. Note that Loop 1 and Loop 2 are fully integrated, meaning that Loop 1 is called to maintain the flux quality at each iteration of Loop 2.

previous local time-steps, i.e.,

$$\eta_{KL}^{(i)} = |F_{e_{KL},\alpha}^{(i)} - F_{e_{KL},\alpha}^{(i-1)}|, \quad (22)$$

where superscript (i) denotes the i -th refinement inside the current global time step, while $(i - 1)$ is the previously accepted time step.

4. Numerical Results

To test the performance of the multirate multiscale method, the numerical test cases presented in [47] are considered. In particular, the top and the bottom layers of the SPE10 test case are used to define the permeability field distribution [54].

The accuracy of the multirate multiscale solution is quantified by comparing it with the one obtained with fine-scale simulation both in space and time (referred to as “reference solution” and denoted with the sub-index “ref”). Pressure relative errors and saturation absolute errors at each point and time are defined as

$$E_P(\mathbf{x}, t) = \frac{|p(\mathbf{x}, t) - p_{ref}(\mathbf{x}, t)|}{|p_{ref}(\mathbf{x}, t)|}, \quad (23)$$

and

$$E_S(\mathbf{x}, t) = |S(\mathbf{x}, t) - S_{ref}(\mathbf{x}, t)|, \quad (24)$$

respectively, where $|\cdot|$ is the absolute value. The relative errors in l^2 -norm at time t are defined as

$$E_{2P}(t) = \frac{\|p(t) - p_{ref}(t)\|_2}{\|p_{ref}(t)\|_2} \quad (25)$$

and

$$E_{2S}(t) = \frac{\|S(t) - S_{ref}(t)\|_2}{\|S_{ref}(t)\|_2}, \quad (26)$$

respectively. Here $\|a\|_2 = \sqrt{\sum_i a_i^2}$.

In the following test cases, a rectangular domain with 220×60 fine cells is considered. Multiscale method imposes 20×12 coarse grid cells. The less viscous fluid (water) is injected at cell (1,1) with a non-dimensional rate of 10 and the more viscous fluid (oil) is produced at cell (220,60), at zero pressure. No-flow conditions are applied at the boundary in all test cases. In all simulations the domain is initially filled with oil, i.e. $S_o^0 = 1$. Quadratic relative permeability functions are employed, i.e., $k_w(S_w) = S_w^2$ and $k_o(S_w) = (1 - S_w)^2$. The viscosity ratio μ_o/μ_w is 10.

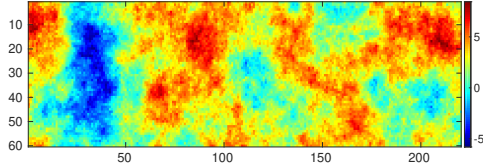


Figure 5: Natural logarithm of the SPE10 top-layer permeability distribution.

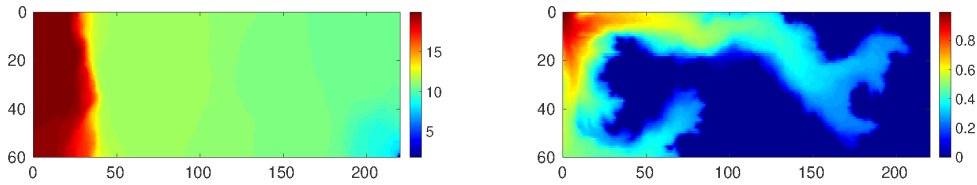


Figure 6: Reference solution maps at final time $t = 600$ for the global pressure (left) and water saturation (right).

4.1. Case 1

The top-layer permeability field of the SPE10 test case, as shown in Figure 5, is considered as Test Case 1. The simulation considers the time interval $[0, 600]$. For $t \in (0, 20)$, a time step size equal to 1 is employed in order to start the multirate computation at $t = 20$ with a well developed saturation profile. The global (coarse-scale) time-step size during the multirate procedure is $\Delta t = 7.25$. The flux quality tolerance and the Newton iterative convergence threshold are set to 10^{-4} and 10^{-8} , respectively. Figure 6 shows the reference solution at final time $t = 600$.

As shown in Figure 7, with the multirate approach only cells near the saturation front are solved at the fine time-scale resolution. These cells are indeed associated with a fast process and sufficiently small time steps are needed to guarantee the required accuracy.

Figure 8 illustrates pressure and saturation errors of simulations computed with coarse time steps and multirate (MR). For both of them, fine-scale grid in space is used. It is clear from this figure that the multirate technique improves the solution, with only a small fraction of the cells at the fine-scale time step. Note that, since pressure and saturation equations are coupled, improving the saturation solution with the multirate method produces a more accurate pressure field.

Figure 9 shows the l^2 -norm of the error of the solutions obtained with the multirate approach and the coarse time steps approach at each global time

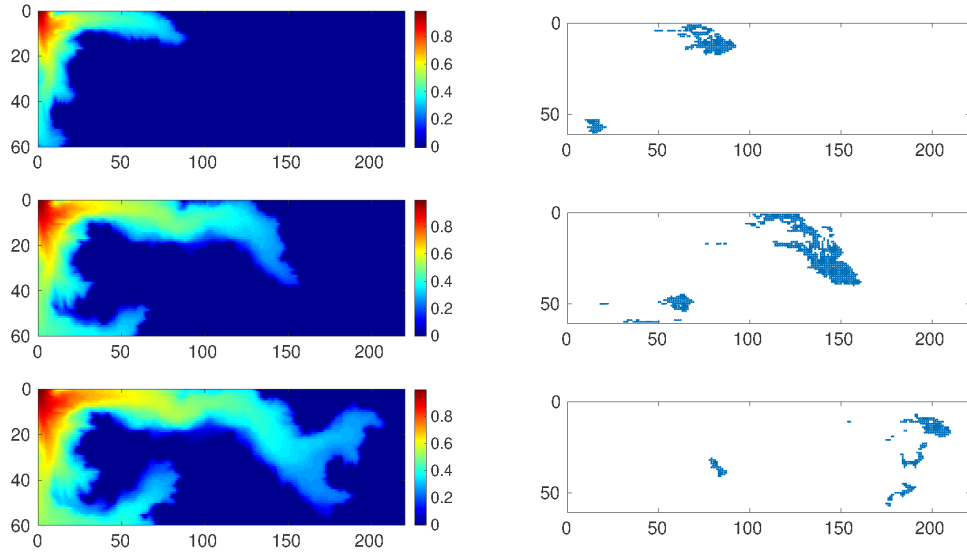


Figure 7: Water saturation solution and active cells at times $t = 222.094$, $t = 435.062$ and $t = 599.094$.

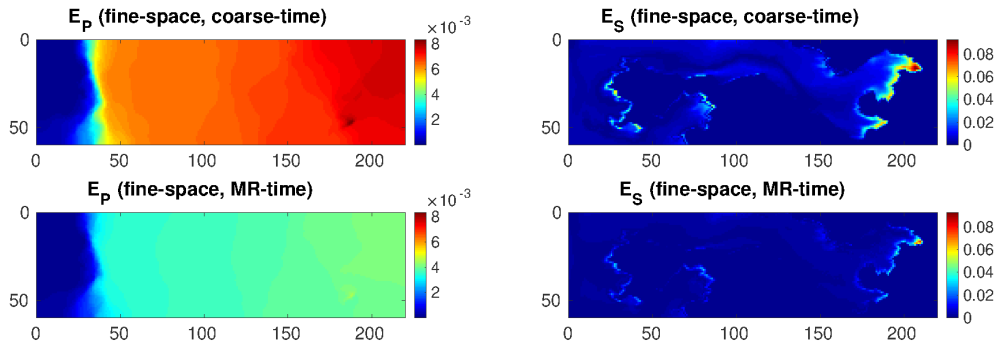


Figure 8: Relative errors for the pressure (left column) and absolute errors for the water saturation (right column) at final time $t = 600$ for the fine space grid, coarse time steps solution (top row) and for the fine space grid, multirate solution (bottom row).

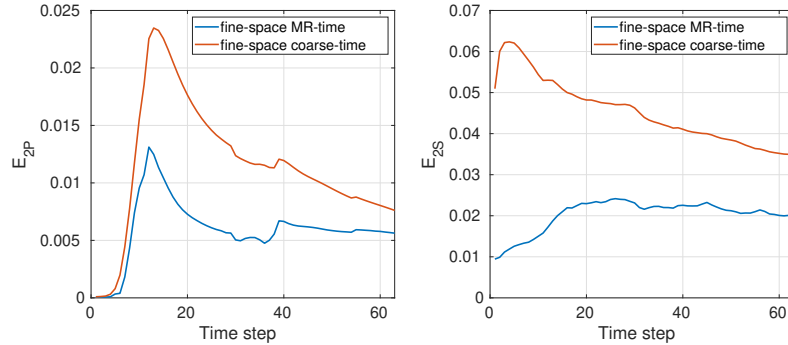


Figure 9: Pressure (left) and saturation (right) relative errors in l^2 -norm at each global step during simulation time for the multirate approach and using only coarse time steps, both computed using the fine space grid.

steps (from time $t = 20$ to time $t = 600$). For both approaches, the solution from $t = 0$ to $t = 20$ is computed using small time steps to start the comparison from an already developed saturation field. The saturation solution with coarse time steps accumulates errors immediately. The multirate approach, however, improves the accuracy of the solution for both the saturation and pressure.

Figure 10 shows that, compared with the single-rate fine time-scale solver, the proposed multirate method applies more Newton iterations to converge to the nonlinear solutions at each global (coarse-scale) time step. This fact motivates the definition of an indicator to estimate the overall computational cost as the cumulative sum of the number of Newton iterations times the number of active components. This indicator is indeed much lower for the multirate solution compared to that obtained single-rate, fine time-step computation. This is because the steps performed with the multirate method with a large Δt require more Newton iterations, as expected. However, this number drops quickly when the sub-critical zones are solved at smaller time step sizes. For this test case, the computational cost of the multirate solution is less than one third that of the fine-scale reference solver (the precise ratio is 0.29).

Figure 11 shows the CFL number associated with the adaptive time steps for multirate simulations, computed using the maximum value of the analytical flux derivative for the saturation. Large portions of the domain (far from the front) exhibit large CFL numbers, while a smaller fraction (near the

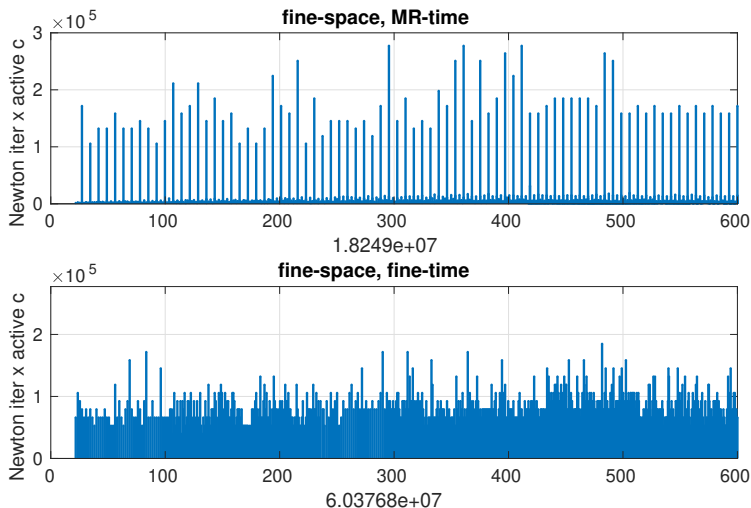


Figure 10: Number of active cells multiplied by the number of Newton iterations at each time step (both global and local) for the multirate (MR) and fine-scale in time solvers. In the x-axis we show the corresponding simulation time. The value presented below each sub-figure is the total complexity of the respective simulation method.

front) advance with smaller CFL numbers. This illustrates the effectiveness of the proposed multirate method. In the simulations, the refinement of the time step is stopped once it leads to $CFL = 0.8$.

Now that the multirate method in time is fully investigated, we combine it with the multiscale method in space. Figure 12 reports the errors of the multiscale in space and coarse time-step (top) solution as well as those obtained with the multiscale multirate approach (bottom). There are no notable differences between the two solutions because the spatial errors introduced by the multiscale procedure dominate the overall errors. In fact, as shown in Figure 13, the errors of the multiscale method with fine time steps are indistinguishable from those reported in Figure 12.

Figure 14 shows the simulation errors, similarly to Figure 12, but with the iterative multiscale solver in space. Here, the two-stage multiscale solver is employed until the l^2 -norm of the pressure residual is equal to 10^{-3} (top) and equal to 10^{-5} (bottom). For both the simulations the number of smoothing per iteration step was set to $n_s = 5$. Consistently with what is reported in the literature, decreasing the pressure residual tolerance results in more accurate pressure and saturation.

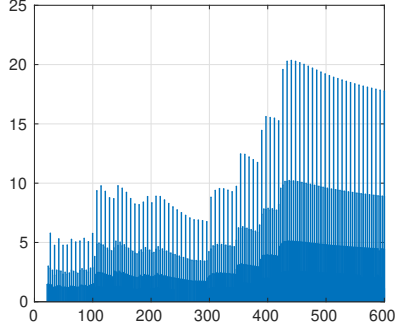


Figure 11: CFL numbers (based on maximum analytical fractional flow derivative value) at each time step of the multirate method.

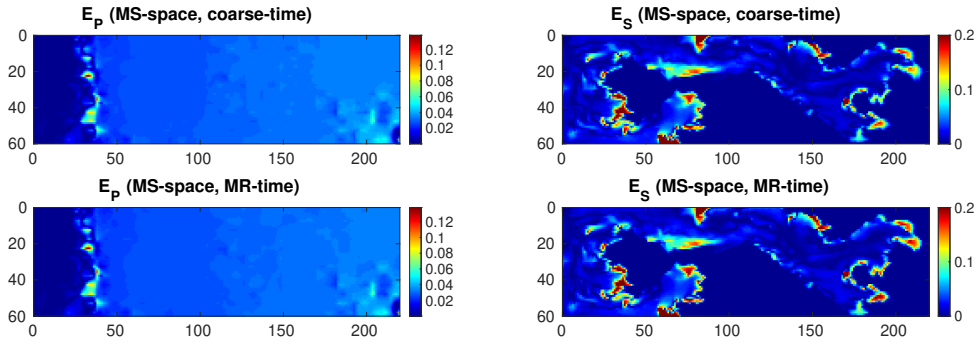


Figure 12: Relative errors for the pressure (left column) and absolute errors for the water saturation (right column) at final time for the multiscale with coarse time steps approach (top row) and for the multirate multiscale method (bottom row).

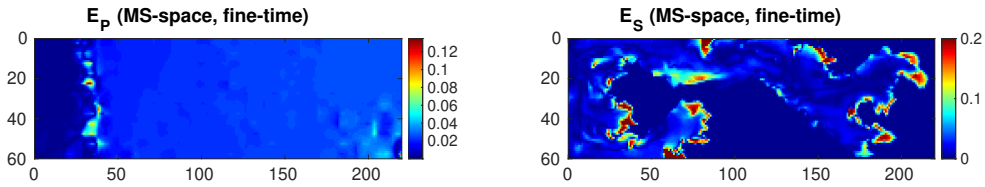


Figure 13: Relative errors for the pressure (left column) and absolute errors for the water saturation (right column) at final time for the multiscale with the fine time steps approach.

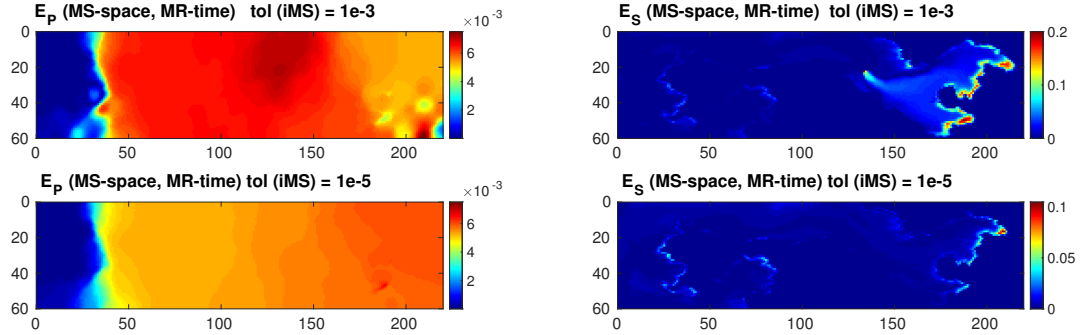


Figure 14: Relative errors for the pressure (left column) and absolute errors for the water saturation (right column) at final time for the multirate iterative multiscale approach with tolerance equal to 10^{-3} (top row) and equal to 10^{-5} (bottom row).

Figure 15 presents the multirate multiscale errors compared with those of multiscale in space single-rate coarse-step in time. It is evident that the multirate method improves the solution by applying fine-scale time-steps only close to the saturation front. This is further elaborated in Figure 16, which reports the l^2 -norm of pressure saturation relative errors at each global time-step. Also in this case fine time-steps equal to 1 are employed for both the approaches in the initial part of the simulation ($t \in (0, 20)$) to have a good initial saturation profile near the injection point. The solution computed with the multirate multiscale approach is more accurate with respect to the solution computed with coarse-scale in time approach.

Finally, the number of Newton iterations multiplied by the number of active cells (complexity) throughout the simulation time is shown in Figure 17. As the fine-scale in space and time (reference) solution is expected to employ the smallest number of Newton loops, the proposed multirate multiscale method is compared with the reference solution. The same speedup for the transport equation solution (i.e., 3 times faster) is obtained using the multirate multiscale method. This means, using multiscale pressure solver (instead of the fine-scale pressure solver) did not deteriorate the multirate transport speedup.

4.2. Case 2

The permeability field of the SPE 10 bottom layer is considered for the Test Case 2, and is shown in Figure 18.

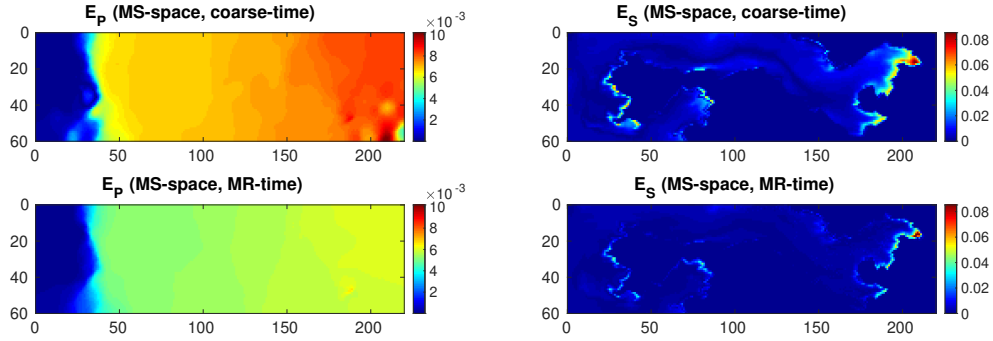


Figure 15: Relative errors for the pressure (left column) and absolute errors for the water saturation (right column) at final time for the coarse time steps (top row) and for the multirate method (bottom row), both considering the iterative multiscale approach with tolerance equal to 10^{-5} .

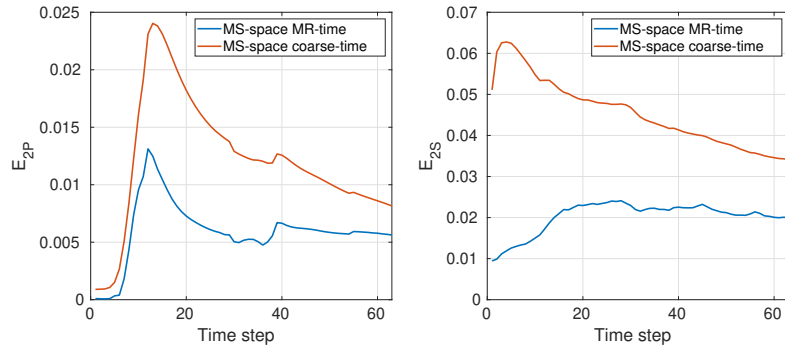


Figure 16: Evolution of pressure (left) and saturation (right) relative errors in l^2 -norm at each global time step for the multirate iterative multiscale approach and the iterative multiscale, coarse time steps approach. The iterative multiscale tolerance is 10^{-5} .

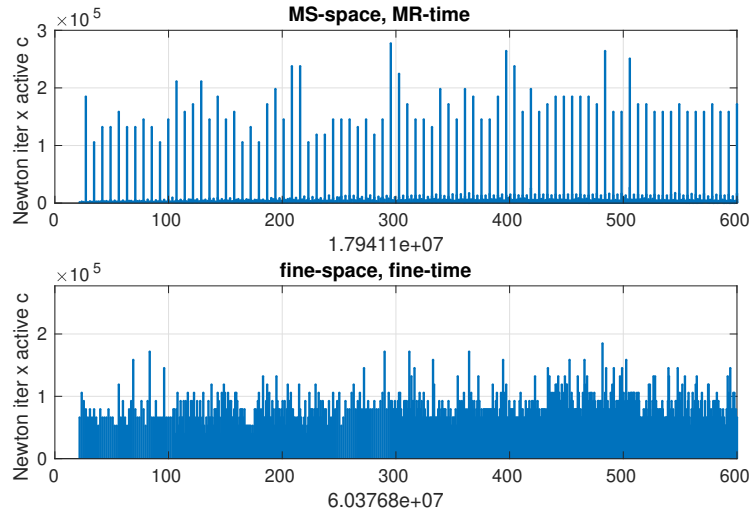


Figure 17: Number of active cells multiplied by the number of Newton iterations at each time step for the multirate multiscale and reference solvers. The iterative multiscale tolerance is 10^{-5} . The value presented below each sub-figure is the total complexity of the respective method.

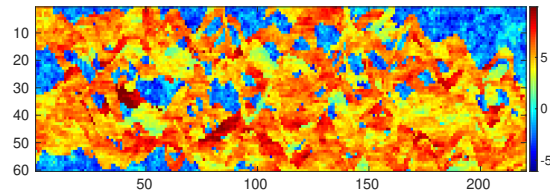


Figure 18: Bottom-layer logarithmic permeability distribution.

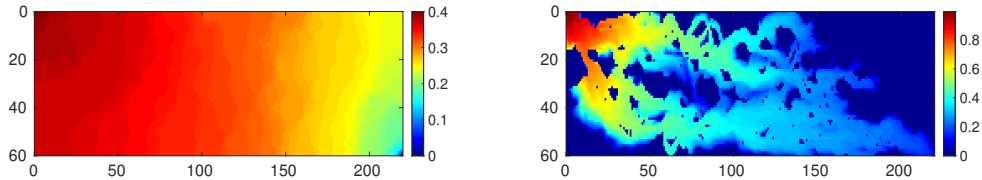


Figure 19: Reference solution of pressure (left) and water saturation (right) at final time $t = 600$.

As in the previous case, the simulation starts at time $t = 0$ and ends at time $t = 600$. The global time step is equal to 5.5 starting from time $t = 5$. In the range $t = (0, 5]$ a fine time step equal to 1 has been employed for all approaches (multirate, fine time-steps and coarse time steps). The flux tolerance for the multirate approach is equal to 10^{-3} and the Newton convergence tolerance is 10^{-8} . Figure 19 shows the reference solution at final time.

Figure 20 illustrates the active cells where the saturation transport equation is solved by the multirate method at a fine time-scale, at three different instants. The method detects regions where the saturation front is moving fast, i.e., where it is necessary to employ smaller time steps.

As in the previous test case, the multirate approach is employed firstly on a fine spatial grid. Figure 21 shows the errors for single-rate coarse time steps (top) and the multirate method (bottom). The multirate technique improves both the pressure error (left) and the saturation error (right). Note that for this challenging case, the coarse time-step solution does not capture the right saturation fronts accurately. The multirate method, instead, leads to a significantly improved solution by employing fine-scale time steps only in the vicinity of the front.

Figure 22 shows the l^2 -norm of pressure and saturation relative errors at each global time-step, starting from time $t = 5$, for both the multirate and overall coarse time-step approaches (using the fine spatial grid in both cases). As expected, the coarse time-step approach is less accurate than the multirate method.

Figure 23 presents the computational complexity of the methods, i.e. the number of Newton iterations multiplied by the number of active cells, for simulations obtained with the multirate (top), fine time-step (center), and coarse time-step (bottom) approaches. The ratio between the computational complexity of the multirate method and that of the reference (fine-scale in space

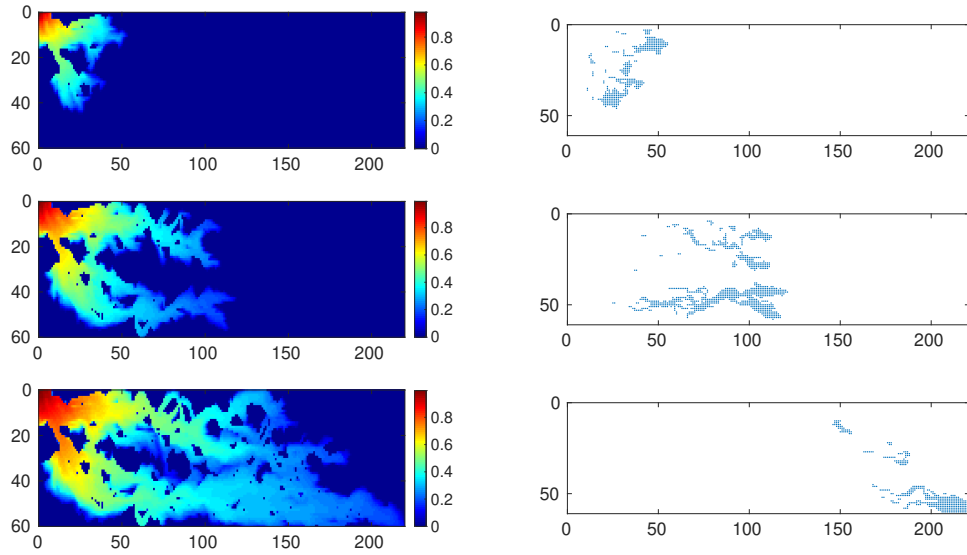


Figure 20: Water saturation solution and active components at times $t = 103.176$, $t = 298.443$ and $t = 599.493$.

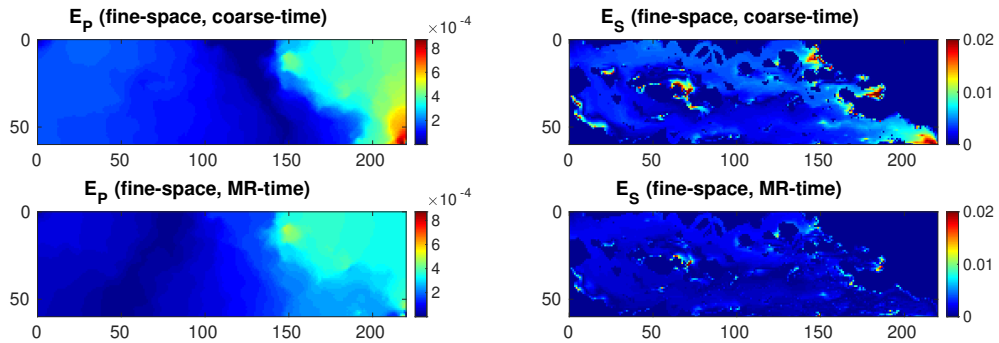


Figure 21: Relative errors for the pressure (left column) and absolute errors for the water saturation (right column) at final time for the coarse time steps solution (top row) and for that obtained with the multirate method (bottom row). Both simulation use the fine spatial grid.

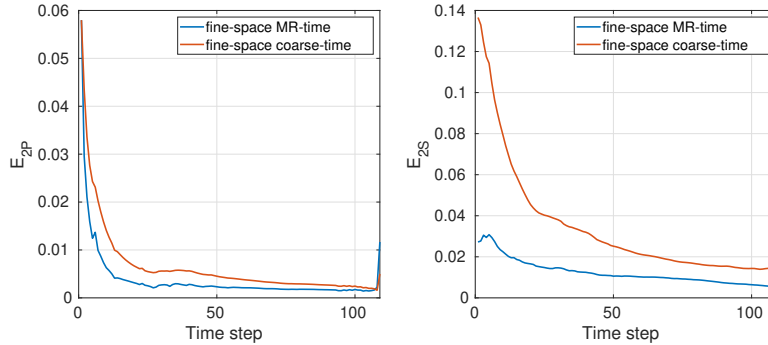


Figure 22: Pressure (left) and saturation (right) relative errors in l^2 -norm during the simulation time for the multirate approach and the coarse time steps approach, both considering the fine space grid.

and time) simulation approach is 0.24. This means the multirate method is almost 4 times faster than the single-rate fine-scale method.

The CFL numbers for the multirate method are given in Figure 24. Also here, the CFL number is computed based on the maximum analytical fractional flow derivative value. Thus, clearly, coarse-scale (global) time steps have rather high CFL values, which makes it attractive for industrial applications.

Finally, the multirate multiscale method is investigated. The iterative multiscale solver tolerance is set to 10^{-6} with $ns = 30$ ILU(0) smoothing steps per iterations. Note that the same global time step size as in the Test Case 1 is used.

Figure 25 illustrates the pressure and saturation errors for the solutions of the iterative multiscale in space and coarse-scale in time (top) and multirate in time (bottom) methods. The results are analogous to those obtained with the fine-scale pressure solver, instead of the multiscale one.

Figure 26 shows the relative errors at the global time steps for the coarse-scale and multirate in time approaches, where both employ the iterative multiscale in space simulation approach. Both the multirate and the single-rate with coarse time steps are performed from time $t = 5$. Also, these results are analogous to the results obtained with the fine-scale (in space) pressure solver.

Finally, Figure 27 shows the number of Newton iterations multiplied by the active (critical sub-domain) cells for the three different approaches. As

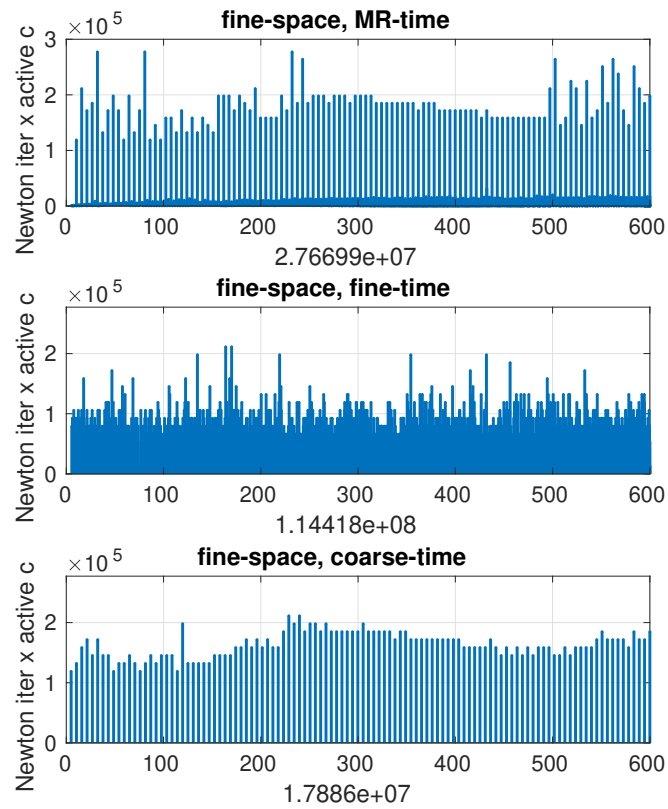


Figure 23: Complexity of the problem: number of Newton iteration per active components required at each time step for the multirate (top), fine time steps (center) and coarse time steps (bottom) approaches. The value presented below each sub-figure is the total complexity of the respective method.

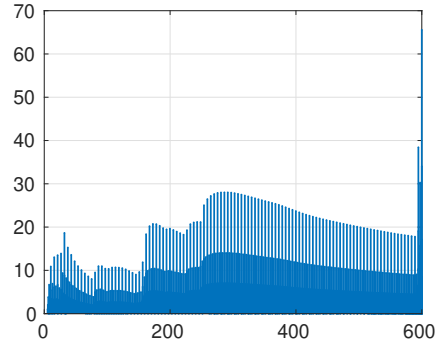


Figure 24: CFL numbers at each time steps for the multirate in time (fine-scale in space) approach.

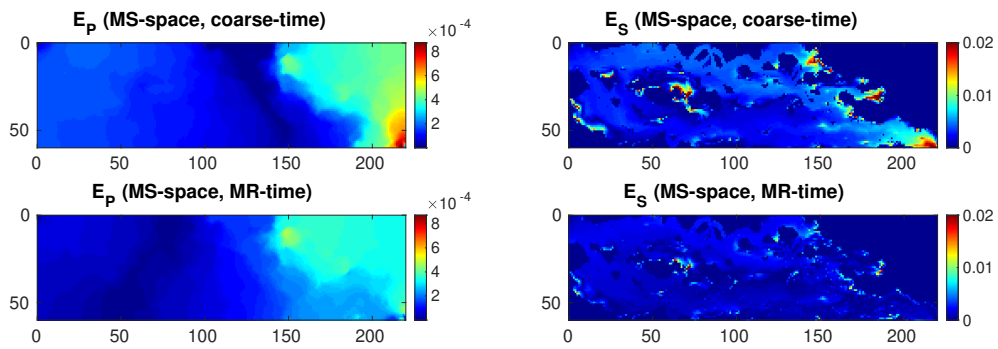


Figure 25: Relative errors for the pressure (left column) and absolute errors for the water saturation (right column) at the final time for the iterative multiscale coarse time steps approach (top row) and for the multirate iterative multiscale approach (bottom row).

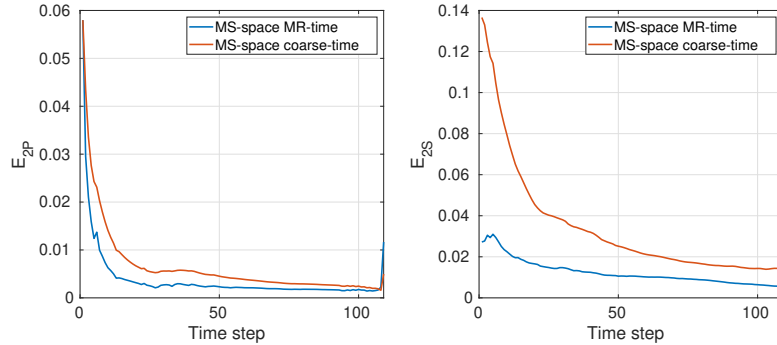


Figure 26: Pressure (left) and saturation (right) relative errors in l^2 -norm during the simulation time for the multirate iterative multiscale approach and the iterative multiscale coarse time steps approach.

in the fine-scale pressure solver approach, the developed multirate method reduces the complexity of the solution obtained from the transport equation by a factor of approximately 4. The error introduced by the multiscale method to solve the pressure equation does not affect the performance of the multirate approach.

5. Conclusions

In this paper, we developed a novel multirate multiscale method for coupled flow and transport equations in heterogeneous porous media. To control the errors in time and space, an iterative multiscale strategy was used to preserve the spatial accuracy coupled with a self-adaptive flux-based refinement strategy for temporal accuracy. The proposed approach has been applied to the implicit pressure implicit saturation approximation of two-phase flow, to have the benefit of large time steps. At the same time, the flux approximation, as well as the iterative multiscale procedure, guarantee the local conservation of mass throughout the simulation.

Proof-of-concept numerical tests show that pressure and saturation solutions improve compared with those obtained from the coarse-scale in time simulations, with only a small fraction of the cells being solved at the fine-scale in time. The investigations include systematic comparisons of both solution error history and computational complexity. Overall, the proposed method allows for advancing the simulation in both space and time accounting for the intrinsic multiscale nature of the problem. As such, it develops a

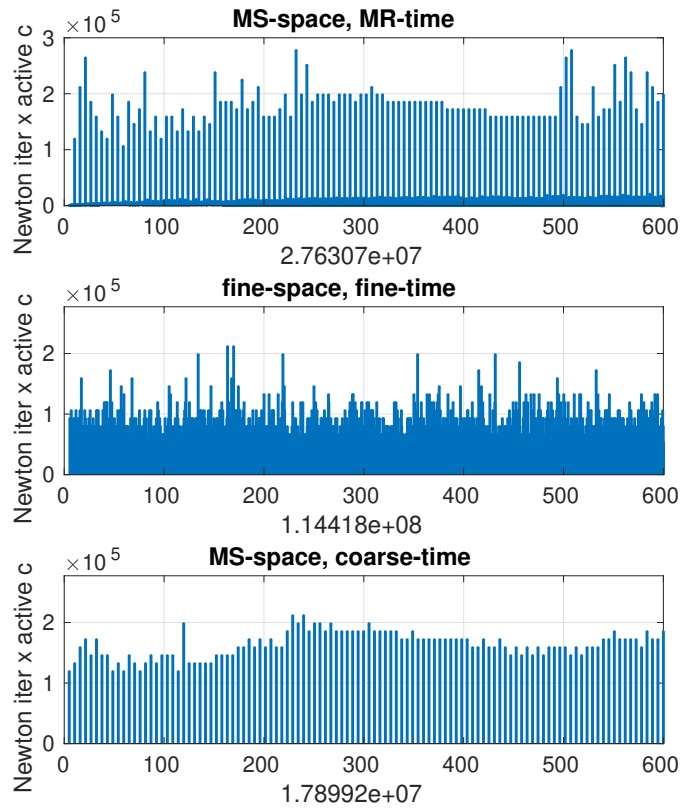


Figure 27: Number of Newton iteration multiplied by the active cells at each time step for the multirate iterative multiscale approach (top), the fine-scale in time and space (center) and the iterative multiscale coarse-scale in time (bottom) approaches. The value presented below each sub-figure is the total complexity of the respective method.

promising simulation approach for large-scale multiphase simulations.

Ongoing research activities include extending the method to adaptive dynamic grid in space with more complex fluid physics, e.g. gravitational and capillary effects.

References

- [1] T. Y. Hou, X.-H. Wu, A multiscale finite element method for elliptic problems in composite materials and porous media, *Journal of computational physics* 134 (1) (1997) 169–189 (1997).
- [2] Y. Efendiev, T. Y. Hou, *Multiscale finite element methods: theory and applications*, Vol. 4, Springer Science & Business Media, 2009 (2009).
- [3] Y. Efendiev, V. Ginting, T. Hou, R. Ewing, Accurate multi-scale finite element methods for two-phase flow simulations, *Journal of Computational Physics* 220 (1) (2006) 155 – 174 (2006). doi:<https://doi.org/10.1016/j.jcp.2006.05.015>.
- [4] P. Jenny, S. Lee, H. Tchelepi, Multi-scale finite-volume method for elliptic problems in subsurface flow simulation, *Journal of Computational Physics* 187 (1) (2003) 47 – 67 (2003).
- [5] H. Hajibeygi, G. Bonfigli, M. A. Hesse, P. Jenny, Iterative multiscale finite-volume method, *Journal of Computational Physics* 227 (19) (2008) 8604 – 8621 (2008).
- [6] J. Aarnes, T. Y. Hou, Multiscale domain decomposition methods for elliptic problems with high aspect ratios, *Acta Mathematicae Applicatae Sinica* 18 (1) (2002) 63–76 (Mar 2002). doi:[10.1007/s102550200004](https://doi.org/10.1007/s102550200004).
- [7] Z. Chen, T. Hou, A mixed multiscale finite element method for elliptic problems with oscillating coefficients, *Mathematics of Computation* 72 (242) (2003) 541–576 (2003).
- [8] V. Kippe, J. E. Aarnes, K.-A. Lie, A comparison of multiscale methods for elliptic problems in porous media flow, *Computational Geosciences* 12 (3) (2008) 377–398 (2008).

- [9] O. Møyner, K.-A. Lie, A multiscale restriction-smoothed basis method for high contrast porous media represented on unstructured grids, *Journal of Computational Physics* 304 (2016) 46 – 71 (2016). doi:<https://doi.org/10.1016/j.jcp.2015.10.010>.
- [10] H. Hajibeygi, P. Jenny, Multiscale finite-volume method for parabolic problems arising from compressible multiphase flow in porous media, *Journal of Computational Physics* 228 (14) (2009) 5129 – 5147 (2009). doi:<https://doi.org/10.1016/j.jcp.2009.04.017>.
- [11] E. T. Chung, Y. Efendiev, W. T. Leung, S. Ye, Generalized multiscale finite element methods for spacetime heterogeneous parabolic equations, *Computers & Mathematics with Applications* 76 (2) (2018) 419 – 437 (2018). doi:<https://doi.org/10.1016/j.camwa.2018.04.028>.
- [12] A. Kozlova, Z. Li, J. R. Natvig, S. Watanabe, Y. Zhou, K. Bratvedt, S. H. Lee, A real-field multiscale black-oil reservoir simulator, *SPE Journal* 21 (06) (2016) 2049–2061 (2016). doi:10.2118/173226-PA.
- [13] S. Lee, C. Wolfsteiner, H. Tchelepi, Multiscale finite-volume formulation for multiphase flow in porous media: black oil formulation of compressible, three-phase flow with gravity, *Computational Geosciences* 12 (3) (2008) 351–366 (2008).
- [14] H. Hajibeygi, H. A. Tchelepi, Compositional multiscale finite-volume formulation, *SPE Journal* 19 (02) (2014) 316–326 (2014). doi:10.2118/163664-PA.
- [15] O. Møyner, K.-A. Lie, A multiscale restriction-smoothed basis method for compressible black-oil models, *SPE Journal* 21 (06) (2016) 2079–2096 (2016). doi:10.2118/173265-PA.
- [16] O. Møyner, H. A. Tchelepi, A mass-conservative sequential implicit multiscale method for isothermal equation-of-state compositional problems, *SPE Journal* 23 (06) (2018) 2376–2393 (2018). doi:10.2118/182679-PA.
- [17] M. Cusini, A. A. Lukyanov, J. Natvig, H. Hajibeygi, Constrained pressure residual multiscale (CPR-MS) method for fully implicit simulation of multiphase flow in porous media, *Journal of Computational Physics* 299 (2015) 472 – 486 (2015). doi:<https://doi.org/10.1016/j.jcp.2015.07.019>.

- [18] M. Cusini, B. Fryer, C. van Kruijsdijk, H. Hajibeygi, Algebraic dynamic multilevel method for compositional flow in heterogeneous porous media, *Journal of Computational Physics* 354 (2018) 593 – 612 (2018). doi:<https://doi.org/10.1016/j.jcp.2017.10.052>.
- [19] T. Praditia, R. Helmig, H. Hajibeygi, Multiscale formulation for coupled flow-heat equations arising from single-phase flow in fractured geothermal reservoirs, *Computational Geosciences* 22 (5) (2018) 1305–1322 (Oct 2018). doi:[10.1007/s10596-018-9754-4](https://doi.org/10.1007/s10596-018-9754-4).
- [20] M. Vasilyeva, M. Babaei, E. T. Chung, D. Spiridonov, Multiscale modeling of heat and mass transfer in fractured media for enhanced geothermal systems applications, *Applied Mathematical Modelling* 67 (2019) 159 – 178 (2019). doi:<https://doi.org/10.1016/j.apm.2018.10.025>.
- [21] H. Hajibeygi, D. Karvounis, P. Jenny, A hierarchical fracture model for the iterative multiscale finite volume method, *Journal of Computational Physics* 230 (24) (2011) 8729–8743 (2011).
- [22] M. Tene, M. S. A. Kobaisi, H. Hajibeygi, Algebraic multiscale method for flow in heterogeneous porous media with embedded discrete fractures (F-AMS), *Journal of Computational Physics* 321 (2016) 819 – 845 (2016). doi:<https://doi.org/10.1016/j.jcp.2016.06.012>.
- [23] S. Bosma, H. Hajibeygi, M. Tene, H. A. Tchelepi, Multiscale finite volume method for discrete fracture modeling on unstructured grids (MS-DFM), *Journal of Computational Physics* 351 (2017) 145 – 164 (2017). doi:<https://doi.org/10.1016/j.jcp.2017.09.032>.
- [24] S. Shah, O. Møyner, M. Tene, K.-A. Lie, H. Hajibeygi, The multiscale restriction smoothed basis method for fractured porous media (F-MsRSB), *Journal of Computational Physics* 318 (2016) 36 – 57 (2016). doi:<https://doi.org/10.1016/j.jcp.2016.05.001>.
- [25] M. Vasilyeva, E. T. Chung, Y. Efendiev, J. Kim, Constrained energy minimization based upscaling for coupled flow and mechanics, *Journal of Computational Physics* 376 (2019) 660 – 674 (2019). doi:<https://doi.org/10.1016/j.jcp.2018.09.054>.

- [26] I. Y. Akkutlu, Y. Efendiev, M. Vasilyeva, Y. Wang, Multiscale model reduction for shale gas transport in poroelastic fractured media, *Journal of Computational Physics* 353 (2018) 356 – 376 (2018). doi:<https://doi.org/10.1016/j.jcp.2017.10.023>.
- [27] I. Lunati, M. Tyagi, S. H. Lee, An iterative multiscale finite volume algorithm converging to the exact solution, *Journal of Computational Physics* 230 (5) (2011) 1849 – 1864 (2011).
- [28] H. Zhou, H. A. Tchelepi, et al., Two-stage algebraic multiscale linear solver for highly heterogeneous reservoir models, *SPE Journal* 17 (02) (2012) 523–539 (2012).
- [29] Y. Wang, H. Hajibeygi, H. A. Tchelepi, Algebraic multiscale solver for flow in heterogeneous porous media, *Journal of Computational Physics* 259 (2014) 284 – 303 (2014).
- [30] M. HosseiniMehr, M. Cusini, C. Vuik, H. Hajibeygi, Algebraic dynamic multilevel method for embedded discrete fracture model (F-ADM), *Journal of Computational Physics* 373 (2018) 324 – 345 (2018). doi:<https://doi.org/10.1016/j.jcp.2018.06.075>.
- [31] R. J. de Moraes, J. J. J. RP. Rodrigues, H. Hajibeygi, Multiscale gradient computation for flow in heterogeneous porous media, *Journal of Computational Physics* 336 (2017) 644–663 (2017).
- [32] J. Jansen, D. Brouwer, G. Naevdal, C. V. Kruijsdijk, Closed-loop reservoir management, *First Break* 23 (2005) 43–48 (2005).
- [33] J. Rice, Split Runge-Kutta methods for simultaneous equations, Vol. 60, *Journal of Research of the National Institute of Standards and Technology*, 1960 (1960).
- [34] G. W. Thomas, D. H. Thurnau, Reservoir simulation using an adaptive implicit method, *Society of Petroleum Engineers Journal* 23 (05) (1983) 759–768 (1983). doi:10.2118/10120-PA.
- [35] D. A. Collins, L. X. Nghiem, Y. K. Li, J. E. Grabonstotter, An efficient approach to adaptive-implicit compositional simulation with an equation of state, *SPE Reservoir Engineering* 7 (02) (1992) 259–264 (1992). doi:10.2118/15133-PA.

- [36] J. Maes, A. Moncorg, H. Tchelepi, Thermal adaptive implicit method: Time step selection, *Journal of Petroleum Science and Engineering* 106 (2013) 34 – 45 (2013). doi:<https://doi.org/10.1016/j.petrol.2013.03.019>.
- [37] P. Forsyth, P. Sammon, Practical considerations for adaptive implicit methods in reservoir simulation, *Journal of Computational Physics* 62 (2) (1986) 265 – 281 (1986). doi:[https://doi.org/10.1016/0021-9991\(86\)90127-0](https://doi.org/10.1016/0021-9991(86)90127-0).
- [38] L. S.-K. Fung, D. A. Collins, L. X. Nghiem, An adaptive-implicit switching criterion based on numerical stability analysis (includes associated paper 18727), *SPE Reservoir Engineering* 4 (01) (1989) 45–51 (1989). doi:[10.2118/16003-PA](https://doi.org/10.1016/0021-9991(86)90127-0).
- [39] J. Moortgat, Adaptive implicit finite element methods for multicomponent compressible flow in heterogeneous and fractured porous media, *Water Resources Research* 53 (2017) 73–92 (2017). doi:[10.1002/2016WR019644](https://doi.org/10.1002/2016WR019644).
- [40] F. Kwok, H. Tchelepi, Potential-based reduced newton algorithm for nonlinear multiphase flow in porous media, *Journal of Computational Physics* 227 (1) (2007) 706 – 727 (2007). doi:<https://doi.org/10.1016/j.jcp.2007.08.012>.
- [41] J. Andrus, Numerical solution of systems of ordinary differential equations separated into subsystems, *SIAM Journal of Numerical Analysis* 16 (1979) 605–611 (1979).
- [42] V. Savcenco, W. Hundsdorfer, J. Verwer, A multirate time stepping strategy for stiff ordinary differential equations, *BIT Numerical Mathematics* 47 (2007) 137–155 (2007).
- [43] E. Constantinescu, A. Sandu, Multirate timestepping methods for hyperbolic conservation laws, *Journal of Scientific Computing* 33 (3) (2007) 239–278 (2007).
- [44] P. Fok, A linearly fourth order multirate Runge–Kutta method with error control, *Journal of Scientific Computing* (2015) 1–19 (2015).

- [45] D. I. Ketcheson, C. B. MacDonald, S. J. Ruuth, Spatially partitioned embedded Runge–Kutta methods, *SIAM Journal on Numerical Analysis* 51 (5) (2013) 2887–2910 (2013).
- [46] L. Delpopolo Carciopolo, L. Bonaventura, A. Scotti, L. Formaggia, A conservative implicit multirate method for hyperbolic problems, *Computational Geosciences* 23 (4) (2019) 647–664 (2019). doi:10.1007/s10596-018-9764-2.
- [47] H. Hajibeygi, S. H. Lee, I. Lunati, et al., Accurate and efficient simulation of multiphase flow in a heterogeneous reservoir with error estimate and control in the multiscale finite-volume framework, *SPE Journal* 17 (04) (2012) 1–071 (2012).
- [48] R. Brooks, T. Corey, Hydraulic properties of porous media, *Hydrology Papers, Colorado State University* 24 (1964) 37 (1964).
- [49] R. Helmig, *Multiphase Flow and Transport Processes in the Subsurface: A Contribution to the Modeling of Hydrosystems*, Springer-Verlag, 1997 (1997).
- [50] K. Aziz, A. Settari, *Petroleum reservoir simulation*, Chapman & Hall, 1979 (1979).
- [51] P. Jenny, H. A. Tchelepi, S. H. Lee, Unconditionally convergent nonlinear solver for hyperbolic conservation laws with S-shaped flux functions, *Journal of Computational Physics* 228 (20) (2009) 7497 – 7512 (2009).
- [52] P. Jenny, I. Lunati, Modeling complex wells with the multi-scale finite-volume method, *Journal of Computational Physics* 228 (2009) 687–702 (2009).
- [53] M. Vohralík, M. F. Wheeler, A posteriori error estimates, stopping criteria, and adaptivity for two-phase flows, *Computational Geosciences* 17 (5) (2013) 789–812 (2013).
- [54] M. Christie, M. Blunt, Tenth SPE comparative solution project: A comparison of upscaling techniques, *SPE Reservoir Simulation Symposium* 11-14 February, 2001 (2001).